

Connectivity Maintenance for Multi-Robot Systems Under Motion and Sensing Uncertainties Using Distributed ADMM-based Trajectory Planning

Akshay Shetty, Derek Knowles and Grace Xingxin Gao

Abstract—Inter-robot communication enables multi-robot systems to coordinate and execute complex missions efficiently. Thus, maintaining connectivity of the communication network between robots is essential for many multi-robot systems. In this paper, we present a trajectory planner for connectivity maintenance of a multi-robot system. Unlike previous connectivity maintenance works, we account for motion and sensing uncertainties inherent in practical robots. These uncertainties result in uncertain robot positions which directly affects the connectivity of the system. We first define a metric to quantify the connectivity of a system with uncertain robot positions. This metric is used to design our trajectory planner based on a distributed alternating direction method of multipliers (ADMM) framework. Next, we derive an approximation for the Hessian matrices required within the ADMM optimization step to reduce the computational load. Finally, simulation results are presented to statistically validate the connectivity maintenance of our trajectory planner.

Index Terms—multi-robot systems, global connectivity maintenance, motion and sensing uncertainties, distributed trajectory planning, alternating direction method of multipliers (ADMM)

I. INTRODUCTION

There has been growing interest in multi-robot systems for exploration [1], [2], target tracking [3], [4], formation control [5]–[7], and cooperative manipulation [8]. Multi-robot systems typically depend on inter-robot communication which enables them to execute complex missions efficiently. Inter-robot communication also adds resilience to malicious attacks [9] and single robot failures [10]. Thus, maintaining connectivity between robots is often a requirement for multi-robot systems.

The topic of connectivity maintenance for multi-robot systems has been widely addressed in literature. The general approach is to synthesize control inputs for each robot in the system such that either local connectivity or global connectivity of the system is maintained [11]. Local connectivity maintenance (LCM) methods focus on keeping the initial topology of connections within the multi-robot system [12]–[17]. Thus, if two robots are initially connected, the synthesized control inputs for these robots maintain their connection throughout the mission. LCM methods typically consist of

relatively simple computations since the control inputs for each robot depend only on local information of the robots to which it is connected. However, the freedom of motion for each robot is restricted since initial connections between robots are not allowed to be broken. Global connectivity maintenance (GCM) methods on the other hand allow individual connections to break as long as there exists a (potentially multi-hop) communication path between any two robots in the system [18]–[27]. Thus, each robot is afforded a greater freedom of motion in comparison to LCM methods.

A limitation of the previous connectivity maintenance works is that they do not explicitly account for motion and sensing uncertainties that are inherent in most practical robots [28]. Presence of motion uncertainty causes the robot to deviate from the trajectory desired by the synthesized control inputs. Additionally, sensing uncertainties result in a robot obtaining a noisy estimate of its own position and its neighbors' positions. These uncertainties consequently result in uncertainty in the robot positions which directly affects the connectivity between robots in the system. Thus, the presence of motion and sensing uncertainties must be accounted for while designing connectivity maintenance methods.

Additionally, the majority of the previous connectivity maintenance works assume a simplified single integrator motion model [19]–[26]. This motion model assumes that the robot position is instantaneously controllable which allows each robot to instantaneously reach the desired position for connectivity maintenance. Thus, these works derive control inputs in a myopic fashion, i.e. only for the current time instant. However, for most practical robots, such as unmanned aerial vehicles (UAVs), the position is not instantaneously controllable. The trajectory that the robot follows typically depends on additional quantities (such as velocity or orientation [29], [30]) and hence the desired position might not be instantaneously reachable. Thus, for connectivity maintenance, it is important to derive control inputs in a non-myopic fashion by considering the trajectory of the robot across multiple time instants.

In this paper, we present a trajectory planning algorithm that maintains the global connectivity of a multi-robot system while accounting for the presence of motion and sensing uncertainties. The main contributions of this paper are listed as follows:

- 1) We define a metric to measure the global connectivity of a multi-robot system with uncertain robot positions arising due to motion and sensing uncertainties. We

Akshay Shetty is with the Department of Aerospace Engineering, University of Illinois at Urbana-Champaign, Champaign, IL, 61801, USA. e-mail: ashetty2@illinois.edu.

Derek Knowles is with the Department of Mechanical Engineering, Stanford University, CA, 94305, USA. e-mail: dcknowles@stanford.edu.

Grace Xingxin Gao is with the Department of Aeronautics and Astronautics, Stanford University, CA, 94305, USA. e-mail: gracegao@stanford.edu.

Manuscript received month xx, 20xx; revised month xx, 20xx.

show that our connectivity metric is a probabilistic lower-bound (with a desired confidence level) for the true algebraic connectivity (explained in Section III) of the system.

- 2) We use the above metric to design a distributed trajectory planning algorithm based on an alternating direction method of multipliers (ADMM) framework [31]. Our algorithm plans trajectories for the system for a specified time horizon while maintaining our connectivity metric above a desired lower limit.
- 3) We analyze the computational load of the optimization step within the ADMM framework. We derive an approximation for the required Hessian matrices which significantly reduces the computational load.
- 4) We simulate multi-UAV missions to statistically validate the global connectivity maintenance of our trajectory planning algorithm. We show the convergence of our planner and evaluate its performance under time constraints.

The remainder of the paper is organized as follows. We begin by discussing related connectivity maintenance works in Section II. Section III provides a background on the relevant topics from graph theory. In Section IV, we formulate the connectivity maintenance and trajectory planning problems for this paper. Section V defines the connectivity metric for uncertain robot positions, which we use in our trajectory planning algorithm detailed in Section VI. We present our simulation results in Section VII and conclude in Section VIII.

II. RELATED WORK: CONNECTIVITY MAINTENANCE

A. Local connectivity maintenance

LCM methods for multi-robot systems are advantageous due to their decentralized nature and their computational simplicity. In [12], the authors introduce a localized notion of connectivity and show that under certain conditions, the global connectivity of the system is also guaranteed. [13] designs a control strategy for the formation control of multi-robot systems while maintaining the initial topology of connections between the robots. In [14], the authors use a potential field-based method for LCM and later extend it to account for robots with bounded control inputs in [15]. The authors in [16] include a repulsive potential field to additionally account for collisions while maintaining local connectivity. [17] builds on the LCM method in [15] to account for critical (close to breaking) initial connections and the presence of leader robots in the system. However, as mentioned in Section I, these works result in less freedom of motion for each robot in the system.

B. Global connectivity maintenance

GCM is widely addressed in literature. A commonly used metric to measure the global connectivity of a multi-robot system is the algebraic connectivity of the graph representing the system. The algebraic connectivity is defined as the second smallest eigenvalue of the graph Laplacian matrix, as discussed later in Section III. In [20], the authors present a decentralized power iteration algorithm for each robot to estimate the algebraic connectivity of the system. This estimate

is then used to design a decentralized gradient-based controller for GCM. [23] and [21] build on the method in [20] by defining a decentralized estimation procedure for algebraic connectivity that is formally guaranteed to be stable. Given the estimation error boundedness, they formally prove that the proposed control law guarantees GCM. Further, in [22] the authors extend their previous GCM works of [23] and [21] by taking into account the presence of an additional (bounded) control input for each robot. [24] extends on [23] and [21] by explicitly accounting for additional inter-robot constraints such as a desired relative distance and inter-robot collisions. In [25], the authors design a GCM method to account for robots with bounded control inputs. They present a theoretical analysis to evaluate the robustness of the proposed method to uncertainties in the robot positions.

Another common approach for GCM is to design optimization-based methods without estimating the value of the algebraic connectivity itself. In [18], the authors find optimal positions for vertices of a graph that maximize the algebraic connectivity. [19] follows a similar approach and derives control inputs for a multi-robot system using a decentralized potential field-based method. In [27], the authors present a differential game-theoretic formulation for maximizing the algebraic connectivity in the presence of a malicious jammer. [26] uses control barrier functions to integrate a GCM requirement with an additional control input for each robot.

While many of these works present decentralized methods with GCM guarantees, they do not explicitly account for robot motion and sensing uncertainties and a majority of them assume a simplified single integrator robot motion model. In this paper, we primarily address these two limitations for GCM of a multi-robot system. In the remainder of the paper, we simply refer to global connectivity as connectivity.

III. BACKGROUND ON GRAPH THEORY

A multi-robot system can be represented as an undirected graph, where each node represents a robot and each edge represents the connection between two robots. Let N be the number of nodes in the graph. The adjacency matrix A of the graph is defined as a $N \times N$ binary matrix such that $A_{ij} = 1$ if nodes i and j are connected and $A_{ij} = 0$ otherwise [32]. The degree of a node d_i represents the number of nodes it is connected to, i.e., $d_i = \sum_{j=1}^N A_{ij}$. These node degrees d_i are then used to define the degree matrix D of the graph as $D = \text{diag}(d_i)$. Given matrices A and D the Laplacian matrix \mathcal{L} of the graph is defined as $\mathcal{L} = D - A$ [33].

As discussed in Section II-B, algebraic connectivity is a commonly used metric to represent the connectivity of multi-robot systems. It is defined as the second-smallest eigenvalue of \mathcal{L} , i.e., if $\lambda_1^{\mathcal{L}} \leq \lambda_2^{\mathcal{L}} \leq \dots \leq \lambda_N^{\mathcal{L}}$ are the eigenvalues of \mathcal{L} , then $\lambda_2^{\mathcal{L}}$ is the algebraic connectivity of the graph. An important property of algebraic connectivity is that it not only gives an indication on whether the graph is connected or not, but it also gives an indication of *how* well-connected the graph is. The value of the algebraic connectivity varies from zero (if the graph is disconnected) to the number nodes in the graph (if the graph is fully connected), i.e. $0 \leq \lambda_2^{\mathcal{L}} \leq N$. Fig. 1 illustrates the algebraic connectivity for different configurations

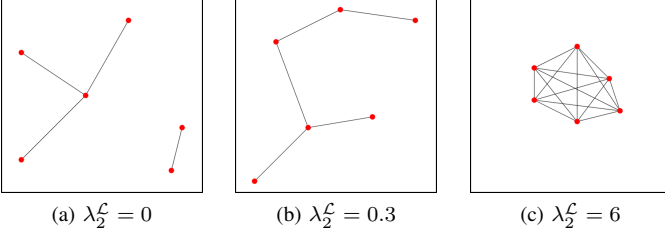


Fig. 1: The algebraic connectivity λ_2^C of a graph varies from zero (disconnected graph) to the number of nodes (fully-connected graph).

of a graph. Thus, λ_2^C remains greater than 0 as long as there exists a (potentially multi-hop) communication path between any two robots in the system.

IV. PROBLEM FORMULATION

A. Robot description

For each robot i in a multi-robot system with N robots, we consider the following nonlinear discrete-time motion and sensing models:

$$\mathbf{x}_{i,t} = \mathbf{f}_i[\mathbf{x}_{i,t-1}, \mathbf{u}_{i,t-1}, \mathbf{w}_{i,t}], \quad (1)$$

$$\mathbf{z}_{i,t} = \mathbf{h}_i[\mathbf{x}_{i,t}, \mathbf{v}_{i,t}], \quad (2)$$

where \mathbf{x}_i is the state vector, \mathbf{u}_i is the input vector, \mathbf{z}_i is the sensed measurement vector, t is the time instant, \mathbf{f}_i is a function representing the motion model, \mathbf{h}_i is a function representing the sensing model, and \mathbf{w}_i and \mathbf{v}_i are Gaussian-distributed error vectors with covariance matrices Q_i and R_i respectively, such that $\mathbf{w}_{i,t} \sim \mathcal{N}[\mathbf{0}, Q_{i,t}]$ and $\mathbf{v}_{i,t} \sim \mathcal{N}[\mathbf{0}, R_{i,t}]$. We assume that each robot implements an extended Kalman filter (EKF) on board to obtain an estimate of its state $\hat{\mathbf{x}}_i$. The prediction step of the EKF is performed as:

$$\bar{\mathbf{x}}_{i,t} = \mathbf{f}_i[\hat{\mathbf{x}}_{i,t-1}, \mathbf{u}_{i,t-1}, \mathbf{0}], \quad (3)$$

$$\bar{\Sigma}_{i,t} = F_{i,t-1} \Sigma_{i,t-1} F_{i,t-1}^\top + Q_{i,t}, \quad (4)$$

where $F_{i,t} = \frac{\partial \mathbf{f}_i}{\partial \mathbf{x}}[\hat{\mathbf{x}}_{i,t}, \mathbf{u}_{i,t}, \mathbf{0}]$ and $\Sigma_{i,t}$ is the state estimation covariance such that $\mathbf{x}_{i,t} \sim \mathcal{N}[\hat{\mathbf{x}}_{i,t}, \Sigma_{i,t}]$. The EKF correction step is performed as:

$$L_{i,t} = \bar{\Sigma}_{i,t} H_{i,t}^\top (H_{i,t} \bar{\Sigma}_{i,t} H_{i,t}^\top + R_{i,t})^{-1}, \quad (5)$$

$$\hat{\mathbf{x}}_{i,t} = \bar{\mathbf{x}}_{i,t} + L_{i,t}(\mathbf{z}_{i,t} - \mathbf{h}_i[\bar{\mathbf{x}}_{i,t}, \mathbf{0}]), \quad (6)$$

$$\Sigma_{i,t} = \bar{\Sigma}_{i,t} - L_{i,t} H_{i,t} \bar{\Sigma}_{i,t}, \quad (7)$$

where $H_{i,t} = \frac{\partial \mathbf{h}_i}{\partial \mathbf{x}}[\bar{\mathbf{x}}_{i,t}, \mathbf{0}]$ and L_i is the Kalman gain. Here the second term in Equation (6) is referred to as the *innovation* term and is distributed according to $\mathcal{N}[\mathbf{0}, L_{i,t} H_{i,t} \bar{\Sigma}_{i,t}]$.

Thus, each robot can be represented in the belief space with the belief vector defined as [34]:

$$\mathbf{b}_{i,t} = \begin{bmatrix} \hat{\mathbf{x}}_{i,t} \\ \mathbf{vec}[\Sigma_{i,t}] \end{bmatrix}, \quad (8)$$

where $\mathbf{vec}[\Sigma_{i,t}]$ denotes a column vector containing the elements of the covariance matrix $\Sigma_{i,t}$. Furthermore, the belief dynamics for the robot can be summarized as [34]:

$$\mathbf{b}_{i,t+1} = \mathbf{g}_i[\mathbf{b}_{i,t}, \mathbf{u}_{i,t}] + M_i[\mathbf{b}_{i,t}, \mathbf{u}_{i,t}] \mathbf{m}_{i,t}, \quad (9)$$

where:

$$\begin{aligned} \mathbf{g}_i[\mathbf{b}_{i,t}, \mathbf{u}_{i,t}] &= \begin{bmatrix} \bar{\mathbf{x}}_{i,t} \\ \mathbf{vec}[\bar{\Sigma}_{i,t} - L_{i,t} H_{i,t} \bar{\Sigma}_{i,t}] \end{bmatrix}, \\ M_i[\mathbf{b}_{i,t}, \mathbf{u}_{i,t}] &= \begin{bmatrix} \sqrt{L_{i,t} H_{i,t} \bar{\Sigma}_{i,t}} \\ 0 \end{bmatrix}, \\ \mathbf{m}_{i,t} &\sim \mathcal{N}[\mathbf{0}, \mathcal{I}], \end{aligned}$$

where \mathcal{I} represents an identity matrix.

B. Connectivity maintenance

The state vector of a robot \mathbf{x}_i typically contains the position of the robot \mathbf{p}_i along with additional quantities such as velocity and orientation. Since we consider a Gaussian distribution for the state vector $\mathbf{x}_{i,t} \sim \mathcal{N}[\hat{\mathbf{x}}_{i,t}, \Sigma_{i,t}]$, the robot positions are also Gaussian-distributed and we represent them as $\mathbf{p}_{i,t} \sim \mathcal{N}[\hat{\mathbf{p}}_{i,t}, P_{i,t}] \forall i \in [1, N]$. Here $\hat{\mathbf{p}}_{i,t}$ is the robot's position estimate which is contained in $\hat{\mathbf{x}}_{i,t}$, and $P_{i,t}$ is the position estimation covariance which is a sub-matrix of $\Sigma_{i,t}$.

Similar to most previous connectivity maintenance works [20]–[25], we assume a disk communication model. Thus, two robots are considered to be connected only if the distance between them is smaller than a specified communication range Δ . Let $l_{ij,t} = \|\mathbf{p}_{i,t} - \mathbf{p}_{j,t}\|_2^2$ be the euclidean distance between two robots i and j , where $\|\cdot\|_2^2$ represents the L2-norm. The corresponding edge weight $A_{ij,t}$ for the adjacency matrix is computed as:

$$A_{ij,t} = \begin{cases} 1 & 0 \leq l_{ij,t} \leq \Delta \\ 0 & l_{ij,t} > \Delta \end{cases}. \quad (10)$$

Given the edge weights, the algebraic connectivity λ_2^C of the multi-robot system is obtained as described earlier in Section III. Note that since the robot positions are stochastic in nature, the algebraic connectivity of the system is also stochastic. Thus, given a lower limit ϵ for the algebraic connectivity, we state the following connectivity maintenance requirement for our trajectory planning algorithm:

$$\Pr[\lambda_2^C > \epsilon] \geq \delta \forall t \in [0, T], \quad (11)$$

i.e., the planner should maintain λ_2^C above ϵ with a minimum probability value of δ for the planning time horizon T . We specify the values of ϵ and δ chosen for our simulations later in Section VII-A.

C. Trajectory planning

The objective of the trajectory planner is to plan nominal trajectories for each robot such that they perform local tasks while maintaining connectivity within the multi-robot system. Here the local tasks can represent objectives such as tracking a target, minimizing the control input effort, avoiding collisions, reaching a desired position for exploration, coverage or formation control, etc. We assume that the following information is available to each robot in the system:

- 1) The initial beliefs of all robots in the system, i.e., $\mathbf{b}_{i,\text{init}} \forall i \in [1, N]$. As defined in Equation (8), the initial belief vector consists of the initial state estimate and the initial estimation covariance.

- 2) The belief dynamics associated with all robots in the system as defined in Equation (9).
- 3) The cost functions representing the local tasks for all robots in the system, i.e., $J_{i,t}[\mathbf{b}_{i,t}, \mathbf{u}_{i,t}] \forall i \in [1, N], \forall t \in [0, T]$.

The nominal trajectory for each robot i can be represented as a series of nominal beliefs and nominal control inputs $(\check{\mathbf{b}}_{i,0}, \check{\mathbf{u}}_{i,0}, \dots, \check{\mathbf{b}}_{i,T-1}, \check{\mathbf{u}}_{i,T-1}, \check{\mathbf{b}}_{i,T})$ [34], such that:

$$\check{\mathbf{b}}_{i,t+1} = \mathbf{g}_i[\check{\mathbf{b}}_{i,t}, \check{\mathbf{u}}_{i,t}] \forall t \in [0, T-1]. \quad (12)$$

We define a concatenated nominal input matrix \check{U} , consisting of nominal input vectors of all robots in the system, over the entire planning time horizon:

$$\check{U} = \begin{bmatrix} \check{\mathbf{u}}_{1,0} & \dots & \check{\mathbf{u}}_{1,T-1} \\ \vdots & \vdots & \vdots \\ \check{\mathbf{u}}_{N,0} & \dots & \check{\mathbf{u}}_{N,T-1} \end{bmatrix}. \quad (13)$$

Note that given the initial beliefs $\mathbf{b}_{i,\text{init}} \forall i \in [1, N]$, it is sufficient to represent the nominal trajectories for the multi-robot system by \check{U} since the nominal beliefs for each robot can be calculated recursively using Equation (12).

Thus, we state the overall objective of the trajectory planner as following:

$$\check{U} = \underset{\check{U}}{\text{argmin}} \sum_{t=0}^T \sum_{i=1}^N J_{i,t}[\check{\mathbf{b}}_{i,t}, \check{\mathbf{u}}_{i,t}], \quad (14)$$

subject to:

$$\Pr[\lambda_2^{\mathcal{L}_t} > \epsilon] \geq \delta \forall t \in [0, T],$$

$$\check{\mathbf{b}}_{i,0} = \mathbf{b}_{i,\text{init}} \forall i \in [1, N],$$

$$\check{\mathbf{b}}_{i,t+1} = \mathbf{g}_i[\check{\mathbf{b}}_{i,t}, \check{\mathbf{u}}_{i,t}] \forall i \in [1, N], \forall t \in [0, T-1],$$

where the first constraint is the connectivity maintenance requirement stated in Equation (11). We use a distributed ADMM-based trajectory planning algorithm to solve the above planning problem as presented later in Section VI.

V. CONNECTIVITY METRIC FOR UNCERTAIN ROBOT POSITIONS

In order to address the connectivity maintenance requirement from Equation (11), we first define a new connectivity metric that accounts for uncertain robot positions arising due to the presence of motion and sensing uncertainties. This metric is then used in our trajectory planning algorithm in Section VI. Since the metric is applicable for any time instant $t \in [0, T]$, for simplicity we omit the time notations in this section.

Given that the position for each robot \mathbf{p}_i is Gaussian-distributed as $\mathbf{p}_i \sim \mathcal{N}[\hat{\mathbf{p}}_i, P_i]$, we begin by considering a confidence ellipse \mathcal{E}_i centered at $\hat{\mathbf{p}}_i$ such that:

$$\Pr[\mathbf{p}_i \in \mathcal{E}_i] = 1 - \delta_\epsilon, \quad (15)$$

where δ_ϵ is a probability value that decides the size of the confidence ellipse. We derive the value for δ_ϵ used in our algorithm later in Equation (25). Let $\bar{\lambda}^{P_i}$ represent the largest eigenvalue of the covariance matrix P_i . Thus, the length of the semi-major axis of \mathcal{E}_i is $s\sqrt{\bar{\lambda}^{P_i}}$, where s is a scalar factor that follows a chi-square distribution [35], [36] based on the

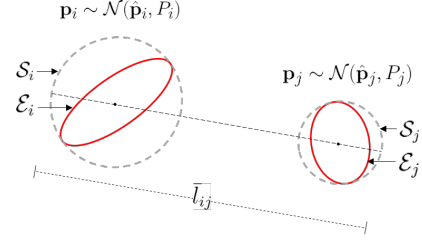


Fig. 2: Distance measure \bar{l}_{ij} between two robots with Gaussian-distributed positions $\mathbf{p}_i \sim \mathcal{N}[\hat{\mathbf{p}}_i, P_i]$ and $\mathbf{p}_j \sim \mathcal{N}[\hat{\mathbf{p}}_j, P_j]$. \bar{l}_{ij} is the maximum distance between the boundaries of the circular regions \mathcal{S}_i and \mathcal{S}_j which overbound the confidence ellipsoids \mathcal{E}_i and \mathcal{E}_j respectively.

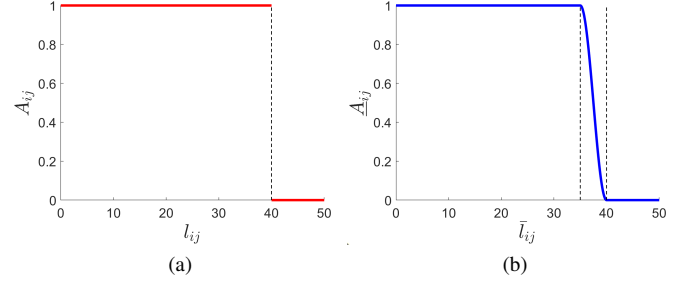


Fig. 3: Edge weights between two robots assuming a communication range of $\Delta = 40$ m. (a) The binary edge weight A_{ij} (Equation 10) is defined as $A_{ij} = 1$ if robots i and j are connected, else $A_{ij} = 0$. (b) For our connectivity metric, we define a non-binary edge weight \bar{A}_{ij} (Equation 18) that gradually goes to 0 as the distance measure \bar{l}_{ij} goes from $\Delta_0 = 35$ m to $\Delta = 40$ m.

value of δ_ϵ . We then define a circular region \mathcal{S}_i centered at $\hat{\mathbf{p}}_i$ with radius $s\sqrt{\bar{\lambda}^{P_i}}$. This circular region overbounds \mathcal{E}_i and thus, contains \mathbf{p}_i with a probability greater than or equal to δ_ϵ , i.e.:

$$\Pr[\mathbf{p}_i \in \mathcal{S}_i] \geq 1 - \delta_\epsilon. \quad (16)$$

We then define a distance measure between the boundaries of the overbounding circular regions of two robots i and j as follows:

$$\bar{l}_{ij} = \|\hat{\mathbf{p}}_i - \hat{\mathbf{p}}_j\|_2^2 + s\sqrt{\bar{\lambda}^{P_i}} + s\sqrt{\bar{\lambda}^{P_j}}. \quad (17)$$

Fig. 2 illustrates the confidence ellipses, the overbounding circular regions and the distance measure between two robots.

Given the communication range of Δ between two robots, we introduce a new parameter Δ_0 , such that $0 < \Delta_0 < \Delta$. Based on the edge weight defined in [24], we use Δ_0 to define a non-binary edge weight between two robots i and j as:

$$\bar{A}_{ij} = \begin{cases} 1 & 0 \leq \bar{l}_{ij} \leq \Delta_0 \\ \frac{1}{2} + \frac{1}{2} \cos \left[\frac{\pi(\bar{l}_{ij} - \Delta_0)}{\Delta - \Delta_0} \right] & \Delta_0 < \bar{l}_{ij} \leq \Delta \\ 0 & \bar{l}_{ij} > \Delta \end{cases}. \quad (18)$$

Fig. 3 compares \bar{A}_{ij} with A_{ij} from Equation (10). We then proceed to define the corresponding degree matrix $\underline{D} = \text{diag}[\underline{d}_i]$ with $\underline{d}_i = \sum_{j=1}^n \bar{A}_{ij}$ and the corresponding Laplacian matrix $\underline{L} = \underline{D} - \underline{A}$. Finally, we use the algebraic connectivity of this graph $\lambda_2^{\underline{L}}$ as our connectivity metric.

Next, we proceed to derive the value of $\delta_{\mathcal{E}}$ required in Equation (15). We define the following events:

$$\begin{aligned}\mathbb{E}_1 &: \mathbf{p}_i \in \mathcal{S}_i \ \forall i \in [1, N], \\ \mathbb{E}_2 &: \bar{l}_{ij} \geq l_{ij} \ \forall \{i, j\} \in [1, N] \times [1, N] \mid i \neq j, \\ \mathbb{E}_3 &: \underline{A}_{ij} \leq A_{ij} \ \forall \{i, j\} \in [1, N] \times [1, N] \mid i \neq j, \\ \mathbb{E}_4 &: \lambda_2^{\mathcal{L}} \geq \lambda_2^{\mathcal{L}}.\end{aligned}$$

Here \mathbb{E}_1 represents the event that all robot positions lie within their corresponding circular regions. We assume that the true positions of the robots in the system are independent of each other. Thus, using Equation (16) we express the probability of event \mathbb{E}_1 as:

$$\Pr[\mathbb{E}_1] = \prod_{i=1}^N \Pr[\mathbf{p}_i \in \mathcal{S}_i] \geq \prod_{i=1}^N (1 - \delta_{\mathcal{E}}) = (1 - \delta_{\mathcal{E}})^N, \quad (19)$$

where N is the number of robots in the system.

\mathbb{E}_2 represents the event that the distance measures \bar{l}_{ij} between any two robots i and j will always be greater than or equal to the true distance l_{ij} . We proceed to derive the probability of event \mathbb{E}_2 as:

$$\begin{aligned}\Pr[\mathbb{E}_2] &= \Pr[\mathbb{E}_2 \mid \mathbb{E}_1] \cdot \Pr[\mathbb{E}_1] + \Pr[\mathbb{E}_2 \mid \mathbb{E}_1'] \cdot \Pr[\mathbb{E}_1'] \\ &\geq \Pr[\mathbb{E}_2 \mid \mathbb{E}_1] \cdot \Pr[\mathbb{E}_1] = \Pr[\mathbb{E}_1],\end{aligned} \quad (20)$$

where $\Pr[\mathbb{E}_2 \mid \mathbb{E}_1] = 1$ since for any two robots i and j if $\mathbf{p}_i \in \mathcal{S}_i$ and $\mathbf{p}_j \in \mathcal{S}_j$, then $\bar{l}_{ij} \geq l_{ij}$ as shown in Fig. 2.

\mathbb{E}_3 represents the event that the non-binary edge weight \underline{A}_{ij} from Equation (18) is less than the edge weight A_{ij} from Equation (10) for any two robots i and j . Similar to Equation (20), we derive the probability of event \mathbb{E}_3 as:

$$\begin{aligned}\Pr[\mathbb{E}_3] &= \Pr[\mathbb{E}_3 \mid \mathbb{E}_2] \cdot \Pr[\mathbb{E}_2] + \Pr[\mathbb{E}_3 \mid \mathbb{E}_2'] \cdot \Pr[\mathbb{E}_2'] \\ &\geq \Pr[\mathbb{E}_3 \mid \mathbb{E}_2] \cdot \Pr[\mathbb{E}_2] = \Pr[\mathbb{E}_2],\end{aligned} \quad (21)$$

where $\Pr[\mathbb{E}_3 \mid \mathbb{E}_2] = 1$ since for any two robots i and j if $\bar{l}_{ij} \geq l_{ij}$, then $\underline{A}_{ij} \leq A_{ij}$ as shown in Fig. 3.

Finally, \mathbb{E}_4 represents the event that our metric $\lambda_2^{\mathcal{L}}$ is less than or equal to the true algebraic connectivity $\lambda_2^{\mathcal{L}}$. The probability of event \mathbb{E}_4 is derived as:

$$\begin{aligned}\Pr[\mathbb{E}_4] &= \Pr[\mathbb{E}_4 \mid \mathbb{E}_3] \cdot \Pr[\mathbb{E}_3] + \Pr[\mathbb{E}_4 \mid \mathbb{E}_3'] \cdot \Pr[\mathbb{E}_3'] \\ &\geq \Pr[\mathbb{E}_4 \mid \mathbb{E}_3] \cdot \Pr[\mathbb{E}_3] = \Pr[\mathbb{E}_3],\end{aligned} \quad (22)$$

where $\Pr[\mathbb{E}_4 \mid \mathbb{E}_3] = 1$ since by definition the algebraic connectivity of a graph monotonically increases as the edge weights in the graph increase [20], [24]. Thus, from Equations (19)-(22) we have:

$$\Pr[\lambda_2^{\mathcal{L}} \geq \lambda_2^{\mathcal{L}}] \geq (1 - \delta_{\mathcal{E}})^N, \quad (23)$$

which shows that our metric $\lambda_2^{\mathcal{L}}$ lower-bounds $\lambda_2^{\mathcal{L}}$ with a minimum probability value of $(1 - \delta_{\mathcal{E}})^N$. If the value of our metric $\lambda_2^{\mathcal{L}}$ is maintained above the specified lower limit ϵ from Equation (14), i.e., if $\lambda_2^{\mathcal{L}} > \epsilon$, then from Equation (23) we get:

$$\Pr[\lambda_2^{\mathcal{L}} > \epsilon] \geq (1 - \delta_{\mathcal{E}})^N. \quad (24)$$

In order to satisfy the connectivity maintenance requirement described in Equation (11), we set $(1 - \delta_{\mathcal{E}})^N = \delta$, which finally gives us the following value for $\delta_{\mathcal{E}}$:

$$\delta_{\mathcal{E}} = 1 - \delta^{(1/N)}, \quad (25)$$

where δ is the probability value representing the desired confidence level in Equation (11).

To summarize, setting the value of $\delta_{\mathcal{E}}$ from Equation (25) and ensuring that our metric $\lambda_2^{\mathcal{L}}$ is maintained above ϵ results in satisfying the connectivity maintenance requirement from Equation (11). Note that our metric definition can be directly extended to three-dimensional, where \mathcal{E}_i (Equation (15)) would represent a confidence ellipsoid for robot i and \mathcal{S}_i (Equation (16)) would represent the corresponding overbounding spherical region.

VI. TRAJECTORY PLANNING ALGORITHM

In this section, we present the details of our trajectory planning algorithm for solving the problem stated in Equation (14). First, we define a connectivity cost function based on our metric $\lambda_2^{\mathcal{L}}$ introduced in Section V. We incorporate this cost function with the cost in Equation (14) to obtain a transformed planning problem. Next, we present a distributed ADMM setup in order to solve the transformed problem and plan nominal trajectories for the multi-robot system. We then describe the method used for performing the optimization step within the ADMM setup and analyze the complexity of its computational bottleneck. Finally, we present an approach to reduce the computational load of this optimization step by deriving an approximation for the required Hessian matrices.

A. Connectivity cost and transformed planning problem

As discussed earlier in Section V, maintaining our metric $\lambda_2^{\mathcal{L}}$ above the lower limit ϵ enables us to satisfy the connectivity maintenance requirement for the multi-robot system as described in Equation (11). Thus, in order to maintain $\lambda_2^{\mathcal{L}}$ above ϵ , we define a connectivity cost function that grows to infinity as $\lambda_2^{\mathcal{L}}$ approaches ϵ . Various cost functions with the above property have been proposed in the related works [21] and [24]. For a distributed ADMM setup, it has been shown that the ADMM iteration complexity is inversely proportional to the algebraic connectivity of the system [37]. Thus, we choose to define the connectivity cost function for any time instant t as following:

$$J_t^c = \frac{k_c}{(\lambda_2^{\mathcal{L}} - \epsilon)} \quad \forall \lambda_2^{\mathcal{L}} > \epsilon, \quad (26)$$

where k_c is a parameter that determines the magnitude of the cost function. Fig. 4 illustrates the connectivity cost function. In order to incorporate the connectivity cost function with Equation (14), we update original planning problem as follows:

$$\tilde{U} = \operatorname{argmin} \left(\sum_{t=0}^T \sum_{i=1}^N J_{i,t}[\tilde{\mathbf{b}}_{i,t}, \tilde{\mathbf{u}}_{i,t}] + \sum_{t=0}^T J_t^c \right) \quad (27)$$

$$= \operatorname{argmin} \sum_{t=0}^T \sum_{i=1}^N \left(J_{i,t}[\tilde{\mathbf{b}}_{i,t}, \tilde{\mathbf{u}}_{i,t}] + \frac{1}{N} J_t^c \right) \quad (28)$$

$$= \operatorname{argmin} \sum_{t=0}^T \sum_{i=1}^N \tilde{J}_{i,t}, \quad (29)$$

where:

$$\tilde{J}_{i,t} = J_{i,t}[\tilde{\mathbf{b}}_{i,t}, \tilde{\mathbf{u}}_{i,t}] + \frac{1}{N} J_t^c.$$

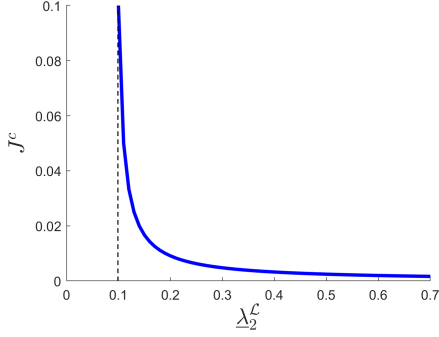


Fig. 4: The connectivity cost function J^c as a function of our connectivity metric λ_2^c (here $k_c = 0.001$). The cost grows to infinity as λ_2^c approaches a specified lower limit of $\epsilon = 0.1$ as shown in Equation (26).

Thus, we write the transformed planning problem as:

$$\begin{aligned} \tilde{U} &= \operatorname{argmin} \sum_{t=0}^T \sum_{i=1}^N \tilde{J}_{i,t} \\ \text{subject to:} \\ \tilde{\mathbf{b}}_{i,0} &= \mathbf{b}_{i,\text{init}} \quad \forall i \in [1, N], \\ \tilde{\mathbf{b}}_{i,t+1} &= \mathbf{g}_i[\tilde{\mathbf{b}}_{i,t}, \tilde{\mathbf{u}}_{i,t}] \quad \forall i \in [1, N], \forall t \in [0, T-1]. \end{aligned} \quad (30)$$

The difference between Equation (14) and the transformed planning problem is that the connectivity maintenance constraint has been incorporated in the cost function. The main reason behind transforming the planning problem from Equation (14) to Equation (30) is to allow us to use existing optimization tools [34] within the ADMM setup, as will be discussed in Section VI-C.

B. Distributed ADMM setup

In order to solve the transformed planning problem from Equation (30), we implement a distributed ADMM setup [31] that iteratively plans nominal trajectories for the multi-robot system. In each ADMM iteration, each robot optimizes only a subset of the robot trajectories in order to reduce the computational load of the optimization step. The optimized trajectories are then communicated with the rest of the system. After the communication step, each robot updates its local ADMM consensus and dual variables before moving on to the next ADMM iteration. Finally, when the stopping criteria is satisfied, the updated local ADMM consensus variable is used as the planned nominal trajectories for the multi-robot system.

Each robot i begins by generating an initial guess for the nominal trajectories of the multi-robot system $\tilde{U}^{(i,1)}$, where the superscript denotes that the variable is stored locally on robot i and is for the first ADMM iteration. The initial guess is typically generated based on the local tasks for each robot. We assume that the process used to generate the initial guess maintains our metric λ_2^c above $\epsilon \forall t \in [0, T]$. Later in Section VII-A, we describe our method for obtaining the initial guess when the local task for each robot involves reaching a desired position. Once the initial guess has been generated, the robot proceeds to initialize its local copy of the consensus variable as

$\bar{U}^{(i,1)} = \tilde{U}^{(i,1)}$. The ADMM dual variable $Y^{(i,1)}$ is initialized as a zero matrix.

Next, the robot begins the ADMM iterations. In each ADMM iteration k , the robot first obtains a subset $\mathcal{V}^{(i,k)}$ containing indices of the robot trajectories to optimize. Different strategies can be deployed for obtaining $\mathcal{V}^{(i,k)}$. For example, setting $\mathcal{V}^{(i,k)} = \{i\}$ results in a greedy optimization where the robot optimizes its own trajectory; setting $\mathcal{V}^{(i,k)}$ to contain neighboring robot indices focuses more on the local connectivity rather than the global connectivity of the system. In our algorithm, we obtain $\mathcal{V}^{(i,k)}$ such that it contains i and cycles through the indices of other robots in the system. Let η represent the number of elements in $\mathcal{V}^{(i,k)}$. Table I shows an example of the subsets $\mathcal{V}^{(i,k)}$ for four ADMM iterations in a system with four robots and with $\eta = 3$. We observe that this strategy for obtaining $\mathcal{V}^{(i,k)}$ avoids the problem of greedy optimizations and eventually results in nominal trajectories for the system with lower overall costs as shown in Section VII.

	$\mathcal{V}^{(1,k)}$	$\mathcal{V}^{(2,k)}$	$\mathcal{V}^{(3,k)}$	$\mathcal{V}^{(4,k)}$
$k = 1$	$\{1, 2, 3\}$	$\{2, 3, 4\}$	$\{3, 4, 1\}$	$\{4, 1, 2\}$
$k = 2$	$\{1, 3, 4\}$	$\{2, 4, 1\}$	$\{3, 1, 2\}$	$\{4, 2, 3\}$
$k = 3$	$\{1, 4, 2\}$	$\{2, 1, 3\}$	$\{3, 2, 4\}$	$\{4, 3, 1\}$
$k = 4$	$\{1, 2, 3\}$	$\{2, 3, 4\}$	$\{3, 4, 1\}$	$\{4, 1, 2\}$

TABLE I: Example of subsets \mathcal{V} for a system with four robots, where $\eta = 3$ and up to $k = 4$ ADMM iterations are considered.

Once the subset $\mathcal{V}^{(i,k)}$ has been obtained, the robot performs the optimization step. In this step, we first initialize $\tilde{U}^{(i,k+1)} = \bar{U}^{(i,k)}$ and then only update the trajectories for robots in the subset $\mathcal{V}^{(i,k)}$. Based on the cost function in Equation (30), the robot optimizes the following augmented cost [31] in order to obtain the optimized trajectories for robots in $\mathcal{V}^{(i,k)}$:

$$\begin{aligned} \tilde{U}_{\mathcal{V}^{(i,k)}}^{(i,k+1)} &= \operatorname{argmin}_{\tilde{U}_{\mathcal{V}^{(i,k)}}} \sum_{t=0}^T \left\{ \sum_{j \in \mathcal{V}^{(i,k)}} \tilde{J}_{j,t} \right. \\ &\quad + \mathbf{y}_{\mathcal{V}^{(i,k)},t}^{(i,k)\top} (\tilde{\mathbf{u}}_{\mathcal{V}^{(i,k)},t} - \bar{\mathbf{u}}_{\mathcal{V}^{(i,k)},t}^{(i,k)}) \\ &\quad \left. + (\rho/2) \left\| \tilde{\mathbf{u}}_{\mathcal{V}^{(i,k)},t} - \bar{\mathbf{u}}_{\mathcal{V}^{(i,k)},t}^{(i,k)} \right\|_2^2 \right\}, \end{aligned} \quad (31)$$

subject to:

$$\begin{aligned} \tilde{\mathbf{b}}_{i,0} &= \mathbf{b}_{i,\text{init}} \quad \forall i \in [1, N], \\ \tilde{\mathbf{b}}_{i,t+1} &= \mathbf{g}_i[\tilde{\mathbf{b}}_{i,t}, \tilde{\mathbf{u}}_{i,t}] \quad \forall i \in [1, N], \forall t \in [0, T-1], \end{aligned}$$

where $\rho > 0$ is the ADMM penalty weight, $\tilde{\mathbf{u}}$ and $\bar{\mathbf{u}}^{(i,k)}$ represent the corresponding vectors from matrices \tilde{U} and $\bar{U}^{(i,k)}$ respectively, and $\mathbf{y}^{(i,k)}$ represents the corresponding vector from dual variable matrix $Y^{(i,k)}$. We discuss the method used to solve this optimization step later in Section VI-C.

After the optimization step, the robot proceeds to the communication step where each robot i shares the optimized trajectories $\tilde{U}_{\mathcal{V}^{(i,k)}}^{(i,k+1)}$ that it obtained from Equation (31). In this step, each robot receives the optimized trajectories from all other robots in the system, potentially via multi-hop communication. Later in Section VII-C, we account for

a delay due to the communication step while evaluating our planner under time constraints. Note that our planner is distributed since each robot optimizes with respect to a subset of trajectories. However, it is not decentralized since each robot shares information with all other robots instead of only its neighbors.

Once the communication step is complete, each robot i receives the optimized trajectories from all other robots. Note that the trajectory for each robot has been optimized η times across the system. For example, in Table I at ADMM iteration $k = 3$, the trajectory for robot 4 was optimized by robots 1, 3 and 4, i.e., $\eta = 3$ times. Thus, based on the consensus update step in [31], the robot calculates an average optimized trajectory for each robot j as follows:

$$\tilde{U}_j^{(i,k+1)} = \frac{1}{\eta} \sum_{l=1}^N \tilde{U}_j^{(l,k+1)} \cdot \mathbb{1}_{\mathcal{V}^{(l,k)}}[j], \quad (32)$$

where $\mathbb{1}_{\mathcal{V}^{(l,k)}}[j]$ is an indicator function equal to 1 if $j \in \mathcal{V}^{(l,k)}$ and equal to 0 otherwise.

After the averaging step, it is possible that $\tilde{U}^{(i,k+1)}$ might result in a trajectory for the multi-robot system that does not maintain our metric $\lambda_2^{\mathcal{L}_t}$ above the lower limit of ϵ . Thus, in order to ensure that the consensus variable \bar{U} always results in trajectories that maintain $\lambda_2^{\mathcal{L}_t} > \epsilon$, we use a line search algorithm [38] to update \bar{U} . We limit the change to \bar{U} between iterations as follows:

$$\bar{U}^{(i,k+1)} = \bar{U}^{(i,k)} + \beta \cdot (\tilde{U}^{(i,k+1)} - \bar{U}^{(i,k)}), \quad (33)$$

where β is a parameter that determines the amount of change in \bar{U} . We begin with $\beta = 1$ and check if the corresponding $\bar{U}^{(i,k+1)}$ results in trajectories that maintain $\lambda_2^{\mathcal{L}_t} > \epsilon$. If $\lambda_2^{\mathcal{L}_t}$ is not maintained above ϵ , we reduce β by a factor γ as: $\beta = \gamma \cdot \beta$, where $0 < \gamma < 1$. We then calculate the new $\bar{U}^{(i,k+1)}$ using Equation (33) and repeat the process until $\bar{U}^{(i,k+1)}$ results in trajectories that maintain $\lambda_2^{\mathcal{L}_t} > \epsilon$. Since our initial nominal trajectory guess maintains $\lambda_2^{\mathcal{L}_t} > \epsilon$, the line search in Equation (33) ensures that \bar{U} always results in trajectories that maintain $\lambda_2^{\mathcal{L}_t} > \epsilon$.

Note that the averaging step in Equation (32) and the consensus update in Equation (33) can be performed on a *central* robot, similar to the approach in [39]. However, dependence on a *central* robot makes the algorithm susceptible to potential single points of failures in the multi-robot system. Additionally, the computational load for Equations (32) and (33) are relatively low since they do not require any optimizations and hence can be quickly performed on every robot. Finally, each robot i updates its ADMM dual variable as follows:

$$Y^{(i,k+1)} = Y^{(i,k)} + \rho \cdot (\tilde{U}^{(i,k+1)} - \bar{U}^{(i,k+1)}), \quad (34)$$

where ρ is the ADMM penalty weight defined in Equation (31).

Before beginning the next ADMM iteration, the robot checks if the stopping criterion has been satisfied. The stopping criteria can be either convergence-based, which is typical for applications when the planning is done in an *offline* manner, or time-based, which is typical for *online* planning

Algorithm 1 Trajectory planner

```

1: for  $i = 1, \dots, N$  do in parallel
2:   Generate initial nominal trajectory guess  $\tilde{U}^{(i,1)}$ 
3:   Initialize consensus variable  $\bar{U}^{(i,1)} = \tilde{U}^{(i,1)}$ , dual
     variable  $Y^{(i,1)}$  as zero matrix, and ADMM iteration  $k = 1$ 
4:   while stopping criterion is not satisfied do
5:     Obtain subset  $\mathcal{V}^{(i,k)}$  of trajectories to optimize
6:     Perform the optimization step (Equation (31)) to
       obtain  $\tilde{U}_{\mathcal{V}^{(i,k)}}^{(i,k+1)}$ 
7:     Communicate  $\tilde{U}_{\mathcal{V}^{(i,k)}}^{(i,k+1)}$  to (and from) other robots
8:     Calculate average optimized trajectories (Equation
       (32)) to obtain  $\tilde{U}^{(i,k+1)}$ 
9:     Update consensus variable  $\bar{U}^{(i,k+1)}$  using line
       search algorithm (Equation (33))
10:    Update dual variable  $Y^{(i,k+1)}$  (Equation (34))
11:    Update ADMM iteration  $k = k + 1$ 
12:   end while
13:   Set planned nominal trajectories as  $\tilde{U} = \bar{U}^{(i,k)}$ 
14: end for

```

applications. If the stopping criteria is satisfied, the robots set the last updated value of \bar{U} as the planned nominal trajectories for the multi-robot system. Since \bar{U} always results in trajectories that maintain $\lambda_2^{\mathcal{L}_t} > \epsilon$, the output from our trajectory planning algorithm always results in trajectories that maintain $\lambda_2^{\mathcal{L}_t} > \epsilon$. Thus, our algorithm satisfies the connectivity maintenance requirement from Equation (11). Algorithm 1 summarizes our trajectory planning algorithm.

C. ADMM trajectory optimization and complexity analysis

In order to obtain the optimized nominal trajectories $\tilde{U}_{\mathcal{V}^{(i,k)}}^{(i,k+1)}$ in Equation (31), we use the belief-space iterative Linear Quadratic Gaussian (belief-space iLQG) method [34]. Since the analysis in the remainder of this section is applicable for a general subset of robot trajectories, we simply represent $\mathcal{V}^{(i,k)}$ as \mathcal{V} . We first extend Equation (9) to define concatenated belief dynamics for the subset \mathcal{V} as follows:

$$\mathbf{b}_{\mathcal{V},t+1} = \mathbf{g}_{\mathcal{V}}[\mathbf{b}_{\mathcal{V},t}, \mathbf{u}_{\mathcal{V},t}] + M_{\mathcal{V}}[\mathbf{b}_{\mathcal{V},t}, \mathbf{u}_{\mathcal{V},t}] \mathbf{m}_{\mathcal{V},t}, \quad (35)$$

where $\mathbf{b}_{\mathcal{V}}$ is the concatenated belief vector of robots in the subset \mathcal{V} . Next, similar to Equation (12), the concatenated nominal trajectory for the subset \mathcal{V} is represented as $(\check{\mathbf{b}}_{\mathcal{V},0}, \check{\mathbf{u}}_{\mathcal{V},0}, \dots, \check{\mathbf{b}}_{\mathcal{V},T-1}, \check{\mathbf{u}}_{\mathcal{V},T-1}, \check{\mathbf{b}}_{\mathcal{V},T})$, such that:

$$\check{\mathbf{b}}_{\mathcal{V},t+1} = \mathbf{g}_{\mathcal{V}}[\check{\mathbf{b}}_{\mathcal{V},t}, \check{\mathbf{u}}_{\mathcal{V},t}] \quad \forall t \in [0, T-1]. \quad (36)$$

Additionally, we rewrite the ADMM optimization step in Equation (31) as:

$$\tilde{U}_{\mathcal{V}}^{(i,k+1)} = \underset{\tilde{U}_{\mathcal{V}}}{\operatorname{argmin}} \sum_{t=0}^T c_t [\check{\mathbf{b}}_{\mathcal{V},t}, \check{\mathbf{u}}_{\mathcal{V},t}], \quad (37)$$

subject to:

$$\begin{aligned} \check{\mathbf{b}}_{\mathcal{V},0} &= \mathbf{b}_{\mathcal{V},\text{init}}, \\ \check{\mathbf{b}}_{\mathcal{V},t+1} &= \mathbf{g}_{\mathcal{V}}[\check{\mathbf{b}}_{\mathcal{V},t}, \check{\mathbf{u}}_{\mathcal{V},t}] \quad \forall t \in [0, T-1], \end{aligned}$$

where c_t is the cost at time instant t . While c_t depends on the belief and input vectors of the entire multi-robot system, for

simplicity we write c_t to be a function of only $\check{\mathbf{b}}_{\mathcal{V}}$ and $\check{\mathbf{u}}_{\mathcal{V}}$ since only the trajectories for subset \mathcal{V} are being optimized. The belief-space iLQG method [34] begins with an initial guess for the nominal trajectory and computes a locally optimal solution for Equation (37) by performing backward value iteration. The value iteration process involves quadratizing the cost function c_t along the nominal trajectory as follows:

$$c_t \approx \frac{1}{2} \begin{bmatrix} \delta \mathbf{b} \\ \delta \mathbf{u} \end{bmatrix}^\top \begin{bmatrix} \check{c}_{\mathbf{b}\mathbf{b},t} & \check{c}_{\mathbf{b}\mathbf{u},t}^\top \\ \check{c}_{\mathbf{u}\mathbf{b},t} & \check{c}_{\mathbf{u}\mathbf{u},t} \end{bmatrix} \begin{bmatrix} \delta \mathbf{b} \\ \delta \mathbf{u} \end{bmatrix} + \begin{bmatrix} \delta \mathbf{b} \\ \delta \mathbf{u} \end{bmatrix}^\top \begin{bmatrix} \check{c}_{\mathbf{b},t} \\ \check{c}_{\mathbf{u},t} \end{bmatrix} + \check{c}_t, \quad (38)$$

where:

$$\begin{aligned} \delta \mathbf{b} &= \mathbf{b}_{\mathcal{V},t} - \check{\mathbf{b}}_{\mathcal{V},t}, & \delta \mathbf{u} &= \mathbf{u}_{\mathcal{V},t} - \check{\mathbf{u}}_{\mathcal{V},t}, \\ \check{c}_{\mathbf{b}\mathbf{b},t} &= \frac{\partial^2 c_t}{\partial \mathbf{b}_{\mathcal{V}} \partial \mathbf{b}_{\mathcal{V}}} [\check{\mathbf{b}}_{\mathcal{V},t}, \check{\mathbf{u}}_{\mathcal{V},t}], & \check{c}_{\mathbf{b}\mathbf{u},t} &= \frac{\partial^2 c_t}{\partial \mathbf{b}_{\mathcal{V}} \partial \mathbf{u}_{\mathcal{V}}} [\check{\mathbf{b}}_{\mathcal{V},t}, \check{\mathbf{u}}_{\mathcal{V},t}], \\ \check{c}_{\mathbf{u}\mathbf{u},t} &= \frac{\partial^2 c_t}{\partial \mathbf{u}_{\mathcal{V}} \partial \mathbf{u}_{\mathcal{V}}} [\check{\mathbf{b}}_{\mathcal{V},t}, \check{\mathbf{u}}_{\mathcal{V},t}], & \check{c}_{\mathbf{b},t} &= \frac{\partial c_t}{\partial \mathbf{b}_{\mathcal{V}}} [\check{\mathbf{b}}_{\mathcal{V},t}, \check{\mathbf{u}}_{\mathcal{V},t}], \\ \check{c}_{\mathbf{u},t} &= \frac{\partial c_t}{\partial \mathbf{u}_{\mathcal{V}}} [\check{\mathbf{b}}_{\mathcal{V},t}, \check{\mathbf{u}}_{\mathcal{V},t}], & \check{c}_t &= c_t [\check{\mathbf{b}}_{\mathcal{V},t}, \check{\mathbf{u}}_{\mathcal{V},t}]. \end{aligned}$$

As discussed in previous works related to belief-space iLQG [4], [34], one of the primary sources of a computational bottleneck lies in the computation of the Hessian $\check{c}_{\mathbf{b}\mathbf{b},t}$. In our trajectory planner, from Equations (27)-(31) and (37), note that the cost function c_t consists of the connectivity cost function J_t^c . Thus, computation of $\check{c}_{\mathbf{b}\mathbf{b},t}$ involves computing the Hessian of the connectivity cost function $\check{J}_{\mathbf{b}\mathbf{b},t}^c = \frac{\partial^2 J_t^c}{\partial \mathbf{b}_{\mathcal{V}} \partial \mathbf{b}_{\mathcal{V}}} [\lambda_2^{\mathcal{L}_t} [\check{\mathbf{b}}_{\mathcal{V},t}]]$. For our belief-space iLQG implementation, we observe that computing $\check{J}_{\mathbf{b}\mathbf{b},t}^c$ is the primary computational bottleneck. Thus, we analyze its complexity below.

For simplicity, we assume that the state vector $\mathbf{x}_{i,t}$ has the same dimension n for all robots in the system throughout the planning horizon. In this case, the dimension of the belief vector for each robot, as defined in Equation (8), is $O[n^2]$ since it contains elements from the state estimation covariance matrix. Thus, the dimension of the concatenated belief vector $\mathbf{b}_{\mathcal{V}}$ is $O[\eta n^2]$, since \mathcal{V} contains η elements. Given the dimension of $\mathbf{b}_{\mathcal{V}}$, the Hessian $\check{J}_{\mathbf{b}\mathbf{b},t}^c$ contains $O[\eta^2 n^4]$ entries. The typical approach to compute the required Hessian in previous belief-space iLQG implementations is to use numerical differentiation (central differences) [4], [34]. Using numerical differentiation would require $O[\eta^2 n^4]$ evaluations of J_t^c , and consequently $O[\eta^2 n^4]$ evaluations of $\lambda_2^{\mathcal{L}_t}$. Considering the entire planning horizon, this results in $O[\eta^2 n^4 T]$ evaluations of $\lambda_2^{\mathcal{L}_t}$ per iteration of belief-space iLQG.

Evaluating $\lambda_2^{\mathcal{L}_t}$ requires obtaining the Laplacian matrix \mathcal{L}_t whose elements depend on the distance measure as shown in Equation (18). For obtaining the distance measures between all robots in the system, we need to perform eigendecompositions of the covariance matrices $P_{i,t} \forall i \in [1, N]$ as shown in Equation (17). Assuming the dimension of the position vector $\mathbf{p}_{i,t}$ to be ϱ , each eigendecomposition can be evaluated in $O[\varrho^3]$ time [40]. Thus, the complexity to obtain \mathcal{L}_t is of $O[\varrho^3 N]$. Once we obtain \mathcal{L}_t , we need to perform another eigendecomposition with complexity of $O[N^3]$ to obtain $\lambda_2^{\mathcal{L}_t}$. Thus, the complexity of a single evaluation of $\lambda_2^{\mathcal{L}_t}$ is of $O[\max[\varrho^3 N, N^3]]$. Given that we need $O[\eta^2 n^4 T]$

evaluations of $\lambda_2^{\mathcal{L}_t}$, we finally have a complexity of $O[\eta^2 n^4 T \cdot \max[\varrho^3 N, N^3]]$ per iteration of belief-space iLQG.

Since we use the belief-space iLQG method for the optimization step within each ADMM iteration, using numerical differentiation to compute $\check{J}_{\mathbf{b}\mathbf{b},t}^c$ results in a prohibitively large computational load. Thus, in the next subsection we present an approach to approximate $\check{J}_{\mathbf{b}\mathbf{b},t}^c$ and consequently reduce the required computational load for the belief-space iLQG method.

D. Hessian approximation for complexity reduction

In this subsection, we drop the time notation for simplicity since the presented approximation is applicable $\forall t \in [0, T]$. As discussed in Section VI-C, the primary computational bottleneck in our implementation of belief-space iLQG arises in computing $\check{J}_{\mathbf{b}\mathbf{b},t}^c$. Thus, in this subsection we derive an analytical expression to approximate $\check{J}_{\mathbf{b}\mathbf{b},t}^c$ and show that it significantly reduces the required computational load.

We begin by obtaining the gradient of our metric $\lambda_2^{\mathcal{L}}$ with respect to the belief vector \mathbf{b}_i as follows [20]:

$$\frac{\partial \lambda_2^{\mathcal{L}}}{\partial \mathbf{b}_i} = (\mathbf{e}_2^{\mathcal{L}})^\top \frac{\partial \mathcal{L}}{\partial \mathbf{b}_i} (\mathbf{e}_2^{\mathcal{L}}) = \sum_{j=1}^N \frac{\partial \mathcal{A}_{ij}}{\partial \mathbf{b}_i} \left(\mathbf{e}_2^{\mathcal{L},(i)} - \mathbf{e}_2^{\mathcal{L},(j)} \right)^2, \quad (39)$$

where $\mathbf{e}_2^{\mathcal{L}}$ is the eigenvector of \mathcal{L} corresponding to the eigenvalue $\lambda_2^{\mathcal{L}}$, and $\mathbf{e}_2^{\mathcal{L},(i)}$ is the i^{th} element of $\mathbf{e}_2^{\mathcal{L}}$. From Equation (18), we obtain the gradient of \mathcal{A}_{ij} with respect to the belief vector \mathbf{b}_i as:

$$\frac{\partial \mathcal{A}_{ij}}{\partial \mathbf{b}_i} = -\frac{\pi}{2(\Delta - \Delta_0)} \sin \left[\frac{\pi(\bar{l}_{ij} - \Delta_0)}{\Delta - \Delta_0} \right] \frac{\partial \bar{l}_{ij}}{\partial \mathbf{b}_i}. \quad (40)$$

Note that while the belief vector \mathbf{b}_i contains the state estimate and the estimation covariance (Equation (8)), the distance measure \bar{l}_{ij} depends only on the position estimate $\hat{\mathbf{p}}_i$ and the position estimation covariance P_i (Equation (17)). Thus, in order to obtain $\frac{\partial \bar{l}_{ij}}{\partial \mathbf{b}_i}$ in Equation (40), we only need the gradient of \bar{l}_{ij} with respect to each element of $\hat{\mathbf{p}}_i$ and with respect to each element of P_i . From Equation (17), the gradient of \bar{l}_{ij} with respect to $\hat{p}_i^{(m)}$, i.e., the m^{th} element of $\hat{\mathbf{p}}_i$, is computed as:

$$\frac{\partial \bar{l}_{ij}}{\partial \hat{p}_i^{(m)}} = \frac{(\hat{p}_i^{(m)} - \hat{p}_j^{(m)})}{\|\hat{\mathbf{p}}_i - \hat{\mathbf{p}}_j\|_2^2}, \quad (41)$$

and the gradient of \bar{l}_{ij} with respect to element (m, b) of P_i is computed as [41]:

$$\frac{\partial \bar{l}_{ij}}{\partial P_i^{(m,b)}} = \left(\frac{s}{2\sqrt{\lambda^{P_i}}} \right) \text{tr} \left[\left(\frac{\partial \bar{\lambda}^{P_i}}{\partial P_i} \right)^\top \left(\frac{\partial P_i}{\partial P_i^{(m,b)}} \right) \right], \quad (42)$$

where $\text{tr}[\cdot]$ represents the trace of a matrix. Furthermore, from [41], we get:

$$\frac{\partial \bar{\lambda}^{P_i}}{\partial P_i} = \frac{(\bar{\mathbf{e}}^{P_i})(\bar{\mathbf{e}}^{P_i})^\top}{(\bar{\mathbf{e}}^{P_i})^\top (\bar{\mathbf{e}}^{P_i})}, \quad (43)$$

where $\bar{\mathbf{e}}^{P_i}$ is the eigenvector of P_i corresponding to the largest eigenvalue $\bar{\lambda}^{P_i}$. Thus, Equation (42) simplifies to:

$$\frac{\partial \bar{l}_{ij}}{\partial P_i^{(m,b)}} = \left(\frac{s}{2\sqrt{\lambda^{P_i}}} \right) \bar{e}^{P_i,(m)} \bar{e}^{P_i,(b)}. \quad (44)$$

Equations (41) and (44) allows us to construct the gradient $\frac{\partial l_{ij}}{\partial \mathbf{b}_i}$, which is required to obtain $\frac{\partial \lambda_2^c}{\partial \mathbf{b}_i}$ using Equations (39) and (40). By concatenating the gradients $\frac{\partial \lambda_2^c}{\partial \mathbf{b}_i} \forall i \in \mathcal{V}$, we obtain the gradient $\frac{\partial \lambda_2^c}{\partial \mathbf{b}_\mathcal{V}}$.

Next, in order to approximate $\check{J}_{\mathbf{b}\mathbf{b}}^c$, we begin by writing the second-order Taylor expansion of J^c about $\check{\mathbf{b}}_\mathcal{V}$:

$$J^c[\lambda_2^c[\mathbf{b}_\mathcal{V}]] \approx \frac{1}{2} \check{J}_{\lambda\lambda}^c (\lambda_2^c[\mathbf{b}_\mathcal{V}] - \lambda_2^c[\check{\mathbf{b}}_\mathcal{V}])^2 + \check{J}_{\lambda}^c (\lambda_2^c[\mathbf{b}_\mathcal{V}] - \lambda_2^c[\check{\mathbf{b}}_\mathcal{V}]) + \check{J}^c, \quad (45)$$

where:

$$\check{J}_{\lambda\lambda}^c = \frac{\partial^2 J^c}{\partial \lambda_2^c \partial \lambda_2^c} [\lambda_2^c[\check{\mathbf{b}}_\mathcal{V}]], \quad \check{J}_{\lambda}^c = \frac{\partial J^c}{\partial \lambda_2^c} [\lambda_2^c[\check{\mathbf{b}}_\mathcal{V}]], \\ \check{J}^c = J^c[\lambda_2^c[\check{\mathbf{b}}_\mathcal{V}]].$$

Here $\check{J}_{\lambda\lambda}^c$ is obtained from Equation (26) as:

$$\check{J}_{\lambda\lambda}^c = \frac{2k_c}{(\lambda_2^c[\check{\mathbf{b}}_\mathcal{V}] - \epsilon)^3}. \quad (46)$$

We then approximate the term $(\lambda_2^c[\mathbf{b}_\mathcal{V}] - \lambda_2^c[\check{\mathbf{b}}_\mathcal{V}])$ in Equation (45) using a first-order Taylor expansion about $\check{\mathbf{b}}_\mathcal{V}$ as follows:

$$\lambda_2^c[\mathbf{b}_\mathcal{V}] - \lambda_2^c[\check{\mathbf{b}}_\mathcal{V}] \approx (\mathbf{b}_\mathcal{V} - \check{\mathbf{b}}_\mathcal{V})^\top \mathbf{a}, \quad (47)$$

where $\mathbf{a} = \left(\frac{\partial \lambda_2^c}{\partial \mathbf{b}_\mathcal{V}} [\check{\mathbf{b}}_\mathcal{V}] \right)^\top$. By substituting Equation (47) in Equation (45), we get:

$$J^c[\lambda_2^c[\mathbf{b}_\mathcal{V}]] \approx \frac{1}{2} (\mathbf{b}_\mathcal{V} - \check{\mathbf{b}}_\mathcal{V})^\top (\check{J}_{\lambda\lambda}^c \mathbf{a} \mathbf{a}^\top) (\mathbf{b}_\mathcal{V} - \check{\mathbf{b}}_\mathcal{V}) + (\mathbf{b}_\mathcal{V} - \check{\mathbf{b}}_\mathcal{V})^\top (\check{J}_{\lambda}^c \mathbf{a}) + \check{J}^c, \quad (48)$$

where $(\check{J}_{\lambda\lambda}^c \mathbf{a} \mathbf{a}^\top)$ is an approximation for $\check{J}_{\mathbf{b}\mathbf{b}}^c$. Note that in order to compute the above approximation for $\check{J}_{\mathbf{b}\mathbf{b}}^c$, we require only a single evaluation of our metric λ_2^c in Equation (46). Considering the entire planning horizon, this results in only T evaluations of λ_2^c per iteration of belief-space iLQG. This is in contrast to using numerical differentiation which requires $O[\eta^2 n^4 T]$ evaluations as discussed in Section VI-C. Thus, approximating $\check{J}_{\mathbf{b}\mathbf{b}}^c$ with $(\check{J}_{\lambda\lambda}^c \mathbf{a} \mathbf{a}^\top)$ significantly reduces the computational load of the belief-space iLQG method.

VII. SIMULATIONS

In this section, we evaluate our trajectory planning algorithm by simulating multiple missions for a multi-UAV system. We first describe the simulation setup which includes the UAV motion and sensing models, the cost functions representing the local tasks, the method used for generating initial trajectory guesses, and the values used for parameters within the planner. We then discuss the performance of our planner for two types of planning applications: *offline* and *online*. For *offline* planning we focus on the convergence of the planner, whereas for *online* planning we focus on the planner performance under time constraints. Additionally, for both applications we statistically validate the connectivity maintenance of our trajectory planning algorithm. All simulations in this section are performed on a 2.80 GHz Quad-core IntelTM i7 machine.

A. Simulation setup

For each UAV in the multi-UAV system, we consider a 2-dimensional (2D) double integrator model as the motion model. The UAV state vector contains the 2D position and velocity, i.e., $\mathbf{x}_{i,t} = [\mathbf{p}_{i,t}^\top \quad \dot{\mathbf{p}}_{i,t}^\top]^\top$, and the input vector is the UAV accelerations. The motion model for the UAV can be written in the form of Equation (1) as:

$$\mathbf{x}_{i,t} = \begin{bmatrix} 1 & 0 & dt & 0 \\ 0 & 1 & 0 & dt \\ 0 & 0 & 1 & 0 \\ 0 & 0 & 0 & 1 \end{bmatrix} \mathbf{x}_{i,t-1} + \begin{bmatrix} \frac{dt^2}{2} & 0 \\ 0 & \frac{dt^2}{2} \\ dt & 0 \\ 0 & dt \end{bmatrix} \mathbf{u}_{i,t-1} + \mathbf{w}_{i,t}, \quad (49)$$

where $dt = 0.2$ s is the time-step between two time instants and

$$\mathbf{w}_{i,t} \sim \mathcal{N} \left[\mathbf{0}, 0.1 \text{ m}^2 \text{s}^{-3} \begin{bmatrix} \frac{dt^3}{3} & 0 & \frac{dt^2}{2} & 0 \\ 0 & \frac{dt^3}{3} & 0 & \frac{dt^2}{2} \\ \frac{dt^2}{2} & 0 & dt & 0 \\ 0 & \frac{dt^2}{2} & 0 & dt \end{bmatrix} \right].$$

Additionally, we set a maximum limit of 5 m s^{-2} on the magnitude of input accelerations. Note that in contrast to a majority of previous connectivity maintenance works, the above motion model does not assume that the UAV positions are instantaneously controllable. For the sensing model in Equation (2), we consider position measurements:

$$\mathbf{z}_{i,t} = \begin{bmatrix} 1 & 0 & 0 & 0 \\ 0 & 1 & 0 & 0 \end{bmatrix} \mathbf{x}_{i,t} + \mathbf{v}_{i,t}, \quad (50)$$

where

$$\mathbf{v}_{i,t} \sim \mathcal{N} \left[\mathbf{0}, \begin{bmatrix} 1 \text{ m}^2 & 0 \\ 0 & 1 \text{ m}^2 \end{bmatrix} \right].$$

Additionally, we assume that each UAV operates at a different altitude, similar to [4]. We make this assumption in order to alleviate inter-UAV collision constraints and focus on the connectivity maintenance of the system.

As mentioned in Section IV-C, each UAV i is considered to have a local task represented by a cost function $J_{i,t}$. For our simulations we consider the local task of reaching a desired position along with minimizing the control input effort. Thus, we use the following cost functions:

$$J_{i,T} = (\hat{\mathbf{x}}_{i,T} - \mathbf{x}_{i,\text{des}})^\top W_i^x (\hat{\mathbf{x}}_{i,T} - \mathbf{x}_{i,\text{des}}), \quad (51)$$

$$J_{i,t} = \mathbf{u}_{i,t}^\top W_i^u \mathbf{u}_{i,t}, \quad (52)$$

where $\mathbf{x}_{i,\text{des}} = [\mathbf{p}_{i,\text{des}}^\top \quad \dot{\mathbf{p}}_{i,\text{des}}^\top]^\top$ contains the desired position $\mathbf{p}_{i,\text{des}}$ and desired velocity $\dot{\mathbf{p}}_{i,\text{des}}$ for the UAV, and W_i^x and W_i^u are used to set the relative importance of the different costs. For our simulations we set $\dot{\mathbf{p}}_{i,\text{des}} = \mathbf{0}$.

We specify an initial position $\mathbf{p}_{i,\text{init}}$ for each UAV i and set their initial velocities to be zeros, i.e., the initial state vector is $\mathbf{x}_{i,\text{init}} = [\mathbf{p}_{i,\text{init}}^\top \quad \mathbf{0}^\top]^\top$. The initial state estimation covariance $\Sigma_{i,\text{init}}$ is set as:

$$\Sigma_{i,\text{init}} = \begin{bmatrix} 0.1 \text{ m}^2 & 0 & 0 & 0 \\ 0 & 0.1 \text{ m}^2 & 0 & 0 \\ 0 & 0 & 0.001 \text{ m}^2 \text{s}^{-2} & 0 \\ 0 & 0 & 0 & 0.001 \text{ m}^2 \text{s}^{-2} \end{bmatrix}. \quad (53)$$

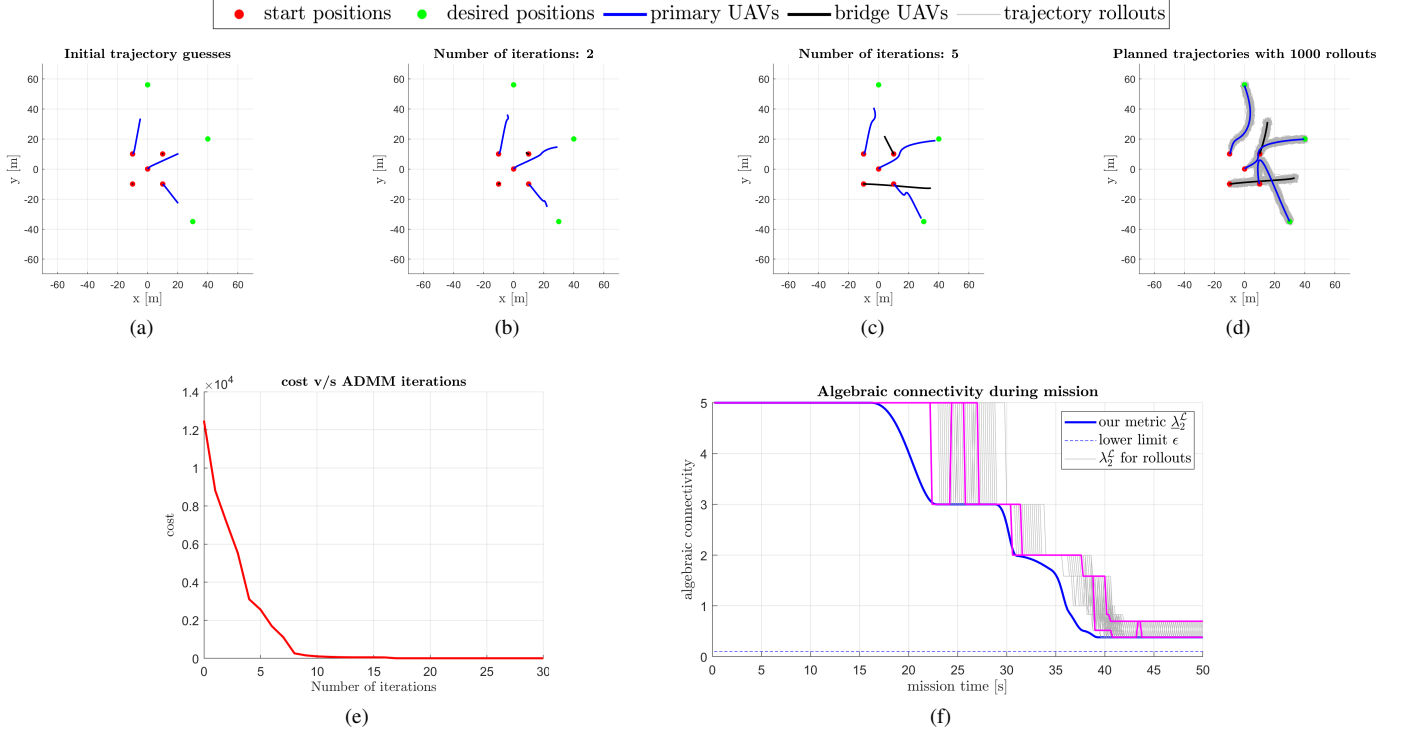


Fig. 5: Trajectory planning and connectivity maintenance for *offline* mission with three *primary* UAVs and two *bridge* UAVs. (a)-(d) Convergence of the planned trajectories. (e) Convergence of the cost in the transformed optimization problem (Equation (30)). (f) Statistical validation of connectivity maintenance throughout the mission. Only two (magenta) of the 1000 trajectory rollouts results in algebraic connectivity λ_2^L less than our metric $\underline{\lambda}_2^L$, whereas none drop below the lower limit ϵ .

For our simulations, we consider the system to be comprised of two types of UAVs: *primary* and *bridge*. The local task for *primary* UAVs includes both reaching the desired position and minimizing control input effort, thus, we set:

$$W_i^{\mathbf{x}} = \begin{bmatrix} 1 & 0 & 0 & 0 \\ 0 & 1 & 0 & 0 \\ 0 & 0 & 100 & 0 \\ 0 & 0 & 0 & 100 \end{bmatrix}, \quad W_i^{\mathbf{u}} = \begin{bmatrix} 0.01 & 0 \\ 0 & 0.01 \end{bmatrix},$$

for each UAV i that is a *primary* UAV. On the other hand, *bridge* UAVs are not assigned a desired position and hence focus on arranging themselves in order to maintain connectivity within the system. Thus for each UAV i that is a *bridge* UAV, we set:

$$W_i^{\mathbf{x}} = \begin{bmatrix} 0 & 0 & 0 & 0 \\ 0 & 0 & 0 & 0 \\ 0 & 0 & 100 & 0 \\ 0 & 0 & 0 & 100 \end{bmatrix}, \quad W_i^{\mathbf{u}} = \begin{bmatrix} 0.01 & 0 \\ 0 & 0.01 \end{bmatrix}.$$

For the initial trajectory guess, we require a computationally inexpensive method of generating a trajectory based on the local tasks for each UAV. For example, sampling-based planners such as rapidly-exploring random trees (RRTs) can be used in order to quickly plan trajectories around obstacles [34], [42]; in a multiple target tracking application, each UAV can be randomly assigned to track a separate target [4]. In our algorithm, we use a linear-quadratic-regulator (LQR) to obtain an initial trajectory guess for each *primary* UAV i from $\mathbf{x}_{i,\text{init}}$ to $\mathbf{x}_{i,\text{des}}$. For *bridge* UAVs, we simply set the initial trajectory guess to be hovering at the initial position. If our metric $\underline{\lambda}_2^L$ is

not maintained above ϵ for the resulting trajectory guess of the multi-UAV system, we consider new desired states (only for the initial trajectory guess and not for the rest of the planner) midway between $\mathbf{x}_{i,\text{init}}$ and the $\mathbf{x}_{i,\text{des}}$ for all *primary* UAVs and repeat the process.

We consider a communication range of $\Delta = 40$ m and set the parameter $\Delta_0 = 35$ m in Equation (18). For the connectivity maintenance requirement in Equation (11), we set the lower algebraic connectivity limit $\epsilon = 0.1$ and the corresponding probability value $\delta = 0.003$ to reflect a 3σ confidence level. We set $T = 250$, which results in a planning time horizon of 50 s. In Equation (26), we set the parameter for the magnitude of the connectivity cost as $k_c = 0.001$. We set $\eta = 2$ for the number of elements in subsets \mathcal{V} obtained in the trajectory planner. Finally, for the line search algorithm used to update the ADMM consensus variable in Equation (33), we set $\gamma = 0.8$.

B. Offline planning

To evaluate our planner for *offline* planning applications, we consider a multi-UAV system with three *primary* UAVs and two *bridge* UAVs. Each *primary* UAV is tasked with reaching a desired position, whereas the *bridge* UAVs are not assigned any desired positions. Fig. 5 shows the results for the *offline* mission. The process of convergence of our trajectory planning algorithm is shown in Figs. 5(a)-(d). As discussed in Section VII-A, for the initial trajectory guess, we use the LQR-based method for the *primary* UAVs, whereas for the *bridge* UAVs we set them to be hovering at their

initial positions. Fig. 5(d) shows the final planned trajectories obtained after the convergence-based stopping criteria has been satisfied. We observe that the final planned trajectories for the *primary* UAVs reach their desired positions, while the *bridge* UAVs arrange themselves in order to maintain connectivity within the system. Additionally, we simulate 1000 trajectory rollouts for the multi-UAV system where each UAV tracks the planned trajectory using LQR. The simulated rollouts are later used to statistically validate the system connectivity. In Fig. 5(e), we show the convergence of the cost in the transformed optimization problem from Equation (30).

Fig. 5(f) shows the connectivity maintenance of the system along the planned trajectories. Given that we incorporated the connectivity cost function (Equation (26)) in the transformed optimization problem (Equation (30)), the planned trajectories maintain our metric λ_2^C above the lower limit ϵ . As discussed in Section V, maintaining $\lambda_2^C > \epsilon$ results in satisfying the connectivity maintenance requirement described in Equation (11). In order to statistically validate that this requirement is satisfied, we compare the algebraic connectivity λ_2^C of the 1000 simulated rollouts against the lower limit ϵ in Fig. 5(f). For only two (colored magenta) of the 1000 rollouts the algebraic connectivity λ_2^C drops below our metric λ_2^C , whereas none drop below the lower limit ϵ . This statistically validates that the connectivity maintenance requirement from Equation (11) is satisfied.

C. Online planning

For *online* planning applications, we evaluate our planning algorithm on a mission under time constraints. We consider the mission to be comprised of multiple segments and allot a maximum planning time for each segment. This resembles applications such as exploration, coverage, or formation control, where only a limited amount of computation time is available for planning trajectories while the remaining time is required for other purposes such as analyzing sensor data or decision making. Given that we consider multiple segments in the mission, we plan the trajectories for the upcoming segment while executing the planned trajectories for the current segment. Fig. 6 shows the order of planning and trajectory execution for the mission. We set a maximum planning time of 25 s and a trajectory duration of 50 s for each segment. Additionally, since our planner potentially requires multi-hop communication, we account for a delay of 0.2 s in each ADMM iteration of our planning algorithm.

We consider a multi-UAV system with ten UAVs: six *primary* and four *bridge*. The *primary* UAVs are tasked with reaching different desired positions in each segment. As shown in Fig. 7 we consider the mission to consist of six segments in order to show the planning results for a variety of configurations of the desired UAV positions. Fig. 7(a) shows the planned trajectories for the first segment along with 1000 trajectory rollouts of the system. The final UAV positions from the first segment are then used as initial positions while planning for the second segment. Figs. 7(b)-(f) show the planned trajectories for the remaining segments. Note that the planner attempts to bring the *primary* UAVs as close as possible to their desired positions while maintaining connectivity of the system.

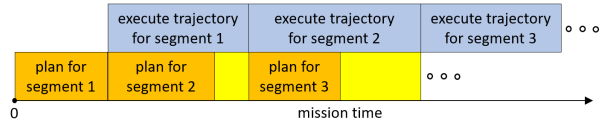


Fig. 6: Order of trajectory planning (orange) and execution (blue) for *online* planning applications. We allot a maximum planning time for each segment since the remaining time (yellow) could be required for other purposes such as analyzing sensor data or decision making.

The convergence of the cost from Equation (30) for the mission segments is shown in Figs. 7(g)-(l). In Fig. 7(m), we show the connectivity maintenance throughout the mission. Note that the order of trajectory planning is as shown in Fig. 6. In Fig. 7(m), we show the connectivity maintenance throughout the mission. Our connectivity metric λ_2^C is maintained above the lower limit ϵ throughout the mission. From the 1000 simulated rollouts, we observe that the algebraic connectivity λ_2^C for only one (colored magenta) rollouts drop below our metric λ_2^C , while none drop below the limit ϵ . Thus, the connectivity maintenance requirement from Equation (11) is satisfied for the *online* mission.

VIII. CONCLUSIONS

We have presented a trajectory planning algorithm for global connectivity maintenance of multi-robot systems. The planner address two limitations in previous connectivity maintenance works: it accounts for robot motion and sensing uncertainties, and it considers robot motion models which do not necessarily have instantaneously controllable positions. To address the connectivity maintenance requirement in the planner, we first define a metric for systems with uncertain robot positions. The metric is then used to define a transformed planning problem which is solved by a distributed ADMM setup. We analyze the complexity of the optimization step within our ADMM setup and present an approach to reduce its computational load by approximating the required Hessian matrices. Finally, we evaluate the planner on simulated *offline* and *online* missions of multi-UAV systems. Our algorithm plans trajectories to complete the local tasks for each UAV while maintaining connectivity within the system. We simulate a 1000 trajectory rollouts for each mission and statistically validate the connectivity maintenance.

REFERENCES

- [1] P. Brass, F. Cabrera-Mora, A. Gasparri, and J. Xiao, "Multirobot Tree and Graph Exploration," *IEEE Transactions on Robotics*, vol. 27, no. 4, pp. 707–717, Aug. 2011.
- [2] W. Burgard, M. Moors, C. Stachniss, and F. E. Schneider, "Coordinated Multi-robot Exploration," *IEEE Transactions on Robotics*, vol. 21, no. 3, pp. 376–386, 2005.
- [3] K. Zhou and S. I. Roumeliotis, "Multirobot Active Target Tracking With Combinations of Relative Observations," *IEEE Transactions on Robotics*, vol. 27, no. 4, pp. 678–695, 2011.
- [4] S.-S. Park, Y. Min, J.-S. Ha, D.-H. Cho, and H.-L. Choi, "A Distributed ADMM Approach to Non-Myopic Path Planning for Multi-Target Tracking," *IEEE Access*, vol. 7, pp. 163 589–163 603, 2019.
- [5] M. Ji and M. Egerstedt, "Distributed Coordination Control of Multiagent Systems While Preserving Connectedness," *IEEE Transactions on Robotics*, vol. 23, no. 4, pp. 693–703, Aug. 2007.

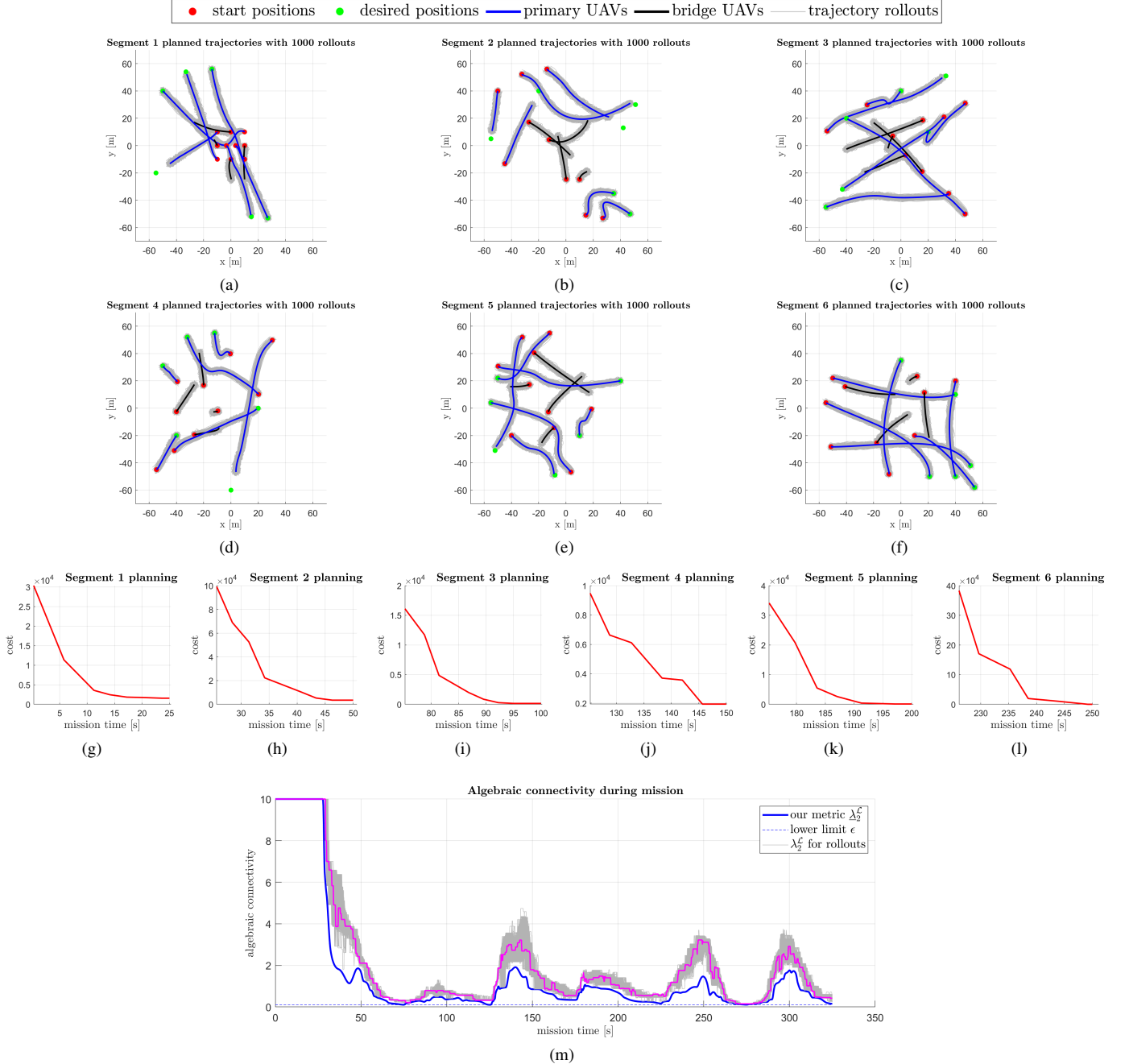


Fig. 7: Trajectory planning and connectivity maintenance for *online* mission with six *primary* and four *bridge* UAVs. (a)-(f) The final planned trajectories and rollouts for each segment of the mission. (g)-(l) Convergence of the cost in the transformed optimization problem for a maximum planning time of 25 s. (m) Statistical validation of connectivity maintenance throughout the mission. Only one (magenta) of the 1000 trajectory rollouts results in algebraic connectivity λ_2^C less than our metric λ_2^C , whereas none drop below the lower limit ϵ .

- [6] M. M. Zavlanos, H. G. Tanner, A. Jadbabaie, and G. J. Pappas, "Hybrid Control for Connectivity Preserving Flocking," *IEEE Transactions on Automatic Control*, vol. 54, no. 12, pp. 2869–2875, dec 2009.
- [7] H. Wang and M. Rubenstein, "Shape Formation in Homogeneous Swarms Using Local Task Swapping," *IEEE Transactions on Robotics*, vol. 36, no. 3, pp. 597–612, 2020.
- [8] P. B. G. Dohmann and S. Hirche, "Distributed Control for Cooperative Manipulation With Event-Triggered Communication," *IEEE Transactions on Robotics*, pp. 1–15, 2020.
- [9] A. Alanwar, H. Said, and M. Althoff, "Distributed Secure State Estimation Using Diffusion Kalman Filters and Reachability Analysis," in *2019 IEEE 58th Conference on Decision and Control (CDC)*. IEEE, 2019, pp. 4133–4139.
- [10] H. Park and S. Hutchinson, "Robust Rendezvous for Multi-robot System with Random Node Failures: An Optimization Approach," *Autonomous Robots*, vol. 42, no. 8, pp. 1807–1818, 2018.
- [11] K. Khateri, M. Pourgholi, M. Montazeri, and L. Sabattini, "A Comparison Between Decentralized Local and Global Methods for Connectivity Maintenance of Multi-robot Networks," *IEEE Robotics and Automation Letters*, vol. 4, no. 2, pp. 633–640, 2019.
- [12] D. P. Spanos and R. M. Murray, "Robust Connectivity of Networked Vehicles," in *2004 43rd IEEE Conference on Decision and Control (CDC)(IEEE Cat. No. 04CH37601)*, vol. 3. IEEE, 2004, pp. 2893–2898.
- [13] Z. Lin, B. Francis, and M. Maggiore, "Necessary and Sufficient Graphical Conditions for Formation Control of Unicycles," *IEEE Transactions*

- on *Automatic Control*, vol. 50, no. 1, pp. 121–127, 2005.
- [14] D. V. Dimarogonas and K. J. Kyriakopoulos, “On the Rendezvous Problem for Multiple Nonholonomic Agents,” *IEEE Transactions on Automatic Control*, vol. 52, no. 5, pp. 916–922, 2007.
 - [15] D. V. Dimarogonas and K. H. Johansson, “Decentralized Connectivity Maintenance in Mobile Networks with Bounded Inputs,” in *2008 IEEE International Conference on Robotics and Automation*. IEEE, 2008, pp. 1507–1512.
 - [16] D. V. Dimarogonas and K. J. Kyriakopoulos, “Connectedness Preserving Distributed Swarm Aggregation for Multiple Kinematic Robots,” *IEEE Transactions on Robotics*, vol. 24, no. 5, pp. 1213–1223, 2008.
 - [17] A. Ajorlou, A. Momeni, and A. G. Aghdam, “A Class of Bounded Distributed Control Strategies for Connectivity Preservation in Multi-agent Systems,” *IEEE Transactions on Automatic Control*, vol. 55, no. 12, pp. 2828–2833, 2010.
 - [18] Y. Kim and M. Mesbahi, “On Maximizing the Second Smallest Eigenvalue of a State-dependent Graph Laplacian,” in *Proceedings of the 2005, American Control Conference*, 2005. IEEE, 2005, pp. 99–103.
 - [19] M. C. De Gennaro and A. Jadbabaie, “Decentralized Control of Connectivity for Multi-agent Systems,” in *Proceedings of the 45th IEEE Conference on Decision and Control*. IEEE, 2006, pp. 3628–3633.
 - [20] P. Yang, R. A. Freeman, G. J. Gordon, K. M. Lynch, S. S. Srinivasa, and R. Sukthankar, “Decentralized Estimation and Control of Graph Connectivity for Mobile Sensor Networks,” *Automatica*, vol. 46, no. 2, pp. 390–396, 2010.
 - [21] L. Sabattini, N. Chopra, and C. Secchi, “Decentralized Connectivity Maintenance for Cooperative Control of Mobile Robotic Systems,” *The International Journal of Robotics Research*, vol. 32, no. 12, pp. 1411–1423, oct 2013. [Online]. Available: <http://journals.sagepub.com/doi/10.1177/0278364913499085>
 - [22] L. Sabattini, C. Secchi, N. Chopra, and A. Gasparri, “Distributed Control of Multirobot Systems with Global Connectivity Maintenance,” *IEEE Transactions on Robotics*, vol. 29, no. 5, pp. 1326–1332, 2013.
 - [23] L. Sabattini, N. Chopra, and C. Secchi, “On Decentralized Connectivity Maintenance for Mobile Robotic Systems,” in *2011 50th IEEE Conference on Decision and Control and European Control Conference*. IEEE, 2011, pp. 988–993.
 - [24] P. Robuffo Giordano, A. Franchi, C. Secchi, and H. H. Bühlhoff, “A Passivity-based Decentralized Strategy for Generalized Connectivity Maintenance,” *The International Journal of Robotics Research*, vol. 32, no. 3, pp. 299–323, 2013.
 - [25] A. Gasparri, L. Sabattini, and G. Ulivi, “Bounded Control Law for Global Connectivity Maintenance in Cooperative Multirobot Systems,” *IEEE Transactions on Robotics*, vol. 33, no. 3, pp. 700–717, 2017.
 - [26] B. Capelli and L. Sabattini, “Connectivity Maintenance: Global and Optimized Approach Through Control Barrier Functions,” *arXiv preprint arXiv:2003.10178*, 2020.
 - [27] S. Bhattacharya and T. Başar, “Graph-theoretic Approach for Connectivity Maintenance in Mobile Networks in the Presence of a Jammer,” in *Proceedings of the IEEE Conference on Decision and Control*, 2010, pp. 3560–3565.
 - [28] S. Thrun, W. Burgard, and D. Fox, “Probabilistic Robotics (Intelligent Robotics and Autonomous Agents series), ser. Intelligent Robotics and Autonomous Agents,” 2005.
 - [29] H. Fernando, A. De Silva, M. De Zoysa, K. Dilshan, and S. Munasinghe, “Modelling, Simulation and Implementation of a Quadrotor UAV,” in *2013 IEEE 8th International Conference on Industrial and Information Systems*. IEEE, 2013, pp. 207–212.
 - [30] M. Owen, R. Beard, and T. McLain, “Implementing Dubins Airplane Paths on Fixed-wing UAVs,” *Contributed chapter to the Handbook of Unmanned Aerial Vehicles*, pp. 1677–1701, 2014.
 - [31] S. Boyd, N. Parikh, E. Chu, J. Eckstein, S. Boyd, N. Parikh, E. Chu, B. Peleato, and J. Eckstein, “Distributed Optimization and Statistical Learning via the Alternating Direction Method of Multipliers,” *Foundations and Trends R in Machine Learning*, vol. 3, no. 1, pp. 1–122, 2010.
 - [32] B. Mohar, Y. Alavi, G. Chartrand, and O. Oellermann, “The Laplacian Spectrum of Graphs,” *Graph theory, Combinatorics, and Applications*, vol. 2, no. 871–898, p. 12, 1991.
 - [33] R. Grone, R. Merris, and V. S. Sunder, “The Laplacian Spectrum of a Graph,” *SIAM Journal on matrix analysis and applications*, vol. 11, no. 2, pp. 218–238, 1990.
 - [34] J. Van Den Berg, S. Patil, and R. Alterovitz, “Motion Planning under Uncertainty using Iterative Local Optimization in Belief Space,” *The International Journal of Robotics Research*, vol. 31, no. 11, pp. 1263–1278, 2012.
 - [35] W. E. Hoover, “Algorithms for Confidence Circles and Ellipses,” *NOAA Technical Report*, 1984.
 - [36] B. Wang, W. Shi, and Z. Miao, “Confidence Analysis of Standard Deviation Ellipse and its Extension into Higher Dimensional Euclidean Space,” *PloS one*, vol. 10, no. 3, p. e0118537, 2015.
 - [37] A. Makhdoumi and A. Ozdaglar, “Convergence Rate of Distributed ADMM over Networks,” *IEEE Transactions on Automatic Control*, vol. 62, no. 10, pp. 5082–5095, 2017.
 - [38] J. J. Moré and D. J. Thuente, “Line Search Algorithms with Guaranteed Sufficient Decrease,” *ACM Transactions on Mathematical Software (TOMS)*, vol. 20, no. 3, pp. 286–307, 1994.
 - [39] B. E. Jackson, T. A. Howell, K. Shah, M. Schwager, and Z. Manchester, “Scalable Cooperative Transport of Cable-Suspended Loads With UAVs Using Distributed Trajectory Optimization,” *IEEE Robotics and Automation Letters*, vol. 5, no. 2, pp. 3368–3374, 2020.
 - [40] V. Y. Pan and Z. Q. Chen, “The Complexity of the Matrix Eigenproblem,” in *Proceedings of the thirty-first annual ACM symposium on Theory of computing*, 1999, pp. 507–516.
 - [41] E. Stump, A. Jadbabaie, and V. Kumar, “Connectivity Management in Mobile Robot Teams,” in *2008 IEEE International Conference on Robotics and Automation*. IEEE, 2008, pp. 1525–1530.
 - [42] G. Gortekin, A. Perez, R. Platt, and G. Konidaris, “Optimal Sampling-based Planning for Linear-quadratic Kinodynamic Systems,” in *2013 IEEE International Conference on Robotics and Automation*. IEEE, 2013, pp. 2429–2436.



Akshay Shetty is a Ph.D. candidate in the Department of Aerospace Engineering at University of Illinois at Urbana-Champaign, and a visiting scholar at Stanford University. He received his M.S. degree in Aerospace Engineering from University of Illinois at Urbana-Champaign in 2017, and his B.Tech. degree in Aerospace Engineering from Indian Institute of Technology, Bombay, India in 2014. His research interests include safety, path planning and control for autonomous vehicles.



Derek Knowles received the B.S. degree in mechanical engineering from Brigham Young University in 2019. He is currently pursuing the M.S. degree in mechanical engineering from Stanford University.

His research interests include autonomous robotic navigation, robust perception, and safe control.



Grace Xingxin Gao is an assistant professor in the Department of Aeronautics and Astronautics at Stanford University. Before joining Stanford University, she was an assistant professor at University of Illinois at Urbana-Champaign. She obtained her Ph.D. degree at Stanford University. Her research is on robust and secure positioning, navigation and timing with applications to manned and unmanned aerial vehicles, robotics and power systems.